UNCLASSIFIED

Defense Technical Information Center
Compilation Part Notice

ADP023736

TITLE: Lattice Boltzmann Algorithms for Fluid Turbulence

DISTRIBUTION: Approved for public release, distribution unlimited

This paper is part of the following report:

TITLE: Proceedings of the HPCMP Users Group Conference 2007. High Performance Computing Modernization Program: A Bridge to Future Defense held 18-21 June 2007 in Pittsburgh, Pennsylvania

To order the complete compilation report, use: ADA488707

The component part is provided here to allow users access to individually authored sections of proceedings, annals, symposia, etc. However, the component should be considered within the context of the overall compilation report and not as a stand-alone technical report.

The following component part numbers comprise the compilation report:
ADP023728 thru ADP023803

UNCLASSIFIED

Lattice Boltzmann Algorithms for Fluid Turbulence

George Vahala
Department of Physics, The College of William and Mary, Williamsburg, VA
vahala@niv.physics.wm.edu

Jeffrey Yepez
US Air Force Research Laboratory (AFRL), Hanscom Field, MA
Jeffrey.Yepez@hanscom.af.mil

Min Soe
Department of Mathematics and Science, Rogers State University, Claremore, OK
MSoe@rsu.edu

Linda Vahala
Department of Electrical & Computer Engineering, Old Dominion University, Norfolk, VA
lvahala@odu.edu

Sean Ziegeler
High Performance Computing Modernization Program, Mississippi State University, MS
seanzig@navo.hpc.mil

Abstract

Lattice Boltzmann algorihms are a mesoscopic representation of nonlinear continuum physics (like Navier-Stokes, magnetohydrodynamics (MHD), Gross-Pitaevskii equations) which are ideal for parallel supercomputers because they transform the difficult nonlinear convective macroscopic derivatives into purely local moments of distribution functions. The macroscopic nonlinearities are recovered by relaxation distribution functions in the collision operator whose dependence on the macroscopic velocity is algebraically nonlinear and thus purely local. Unlike standard computational fluid dynamics codes, there is no loss in parallelization in handling arbitrary geometric boundaries, e.g., using bounce-back rules from kinetic theory. By encoding detailed balance into the collision operator through the introduction of discrete H-function, the lattice Boltzmann algorithm can be made unconditionally stable for arbitrary high Reynolds numbers. It is shown that this approach is a special case of a quantum lattice Boltzmann algorithm that entangles local qubits through unitary collision operators and which is ideally parallelized on quantum computer architectures. Here we consider turbulence simulations using 2,048 PEs on a $1,600^3$-spatial grid. A connection is found between the rate of change of enstrophy and the onset of laminar-to-turbulent flows.

1. Introduction

There is much interest in the defense community to accurately determine turbulent flows over non-trivial boundaries (e.g., instabilities and wakes from naval ships and aircraft) as well as intermittent turbulence induced in the upper atmosphere under the jet stream to optimize laser propagation from airborne platforms. However, for many of these turbulent flows, standard computational fluid dynamics (CFD) codes (now necessarily non-pseudo spectral) quickly saturate with the number of processing elements (PEs) due to the nonlocal nonlinear convective derivatives in the Navier-Stokes equations. However, by projecting into a lattice kinetic phase space, the turbulent dynamics in this mesoscopic description are simpler and much easier to solve with algorithms that are ideally parallelized. The lattice kinetic solution is then projected back into the macroscopic space by Chapman-Enksog expansions to recover the fluid turbulence solution.

The standard lattice Boltzmann (LB) scheme employs a simple Bhatnagar-Gross-Krook (BGK) collision operator, with fixed relaxation rate. This leads to strong numerical instabilities for high Reynolds number flows. However, by enforcing detailed balance[1,2] into the collision operator, a generalized (entropic) BGK operator is found that will lead to unconditionally stable numerical algorithm for arbitrary high Reynolds numbers. Here, we test this entropic lattice scheme (which in some sense can be viewed as a

0-7695-3088-5/07 $25.00 © 2007 IEEE

large eddy simulation) on extremely large grids and determine some of the turbulence statistics. In Section 2, we give a brief overview of the entropic lattice Boltzmann scheme and show its connection to quantum lattice algorithms[3]. In Section 3 we present some of our free shear turbulence simulation results from the Capability Applications Project (CAP) runs using 2,048 PEs on $1{,}600^3$-spatial grids. In Section 4 we discuss a new turbulence morphology gleaned from detailed analysis of simulations on 512^3-grids and present some concluding remarks in Section 5.

2. Lattice Boltzmann Algorithms

At each space-time grid point $(\mathbf{x},t)$ in lattice algorithms, the excited state of a qubit $|q\rangle$ encodes the probability f_q of the existence of a mesoparticle moving with discrete lattice velocity $\mathbf{c}_q = \Delta\mathbf{x}_q / \Delta t$. $\Delta\mathbf{x}_q$ are the lattice vector links, with $q = 1,2, \ldots. Q$, where Q is the number of qubits at each spatial node. The particle momentum is determined from a suitably chosen qubit-qubit interaction Hamiltonian H' while the spatial location arises from the free-streaming Hamiltonian $-i\hbar\sum_q \mathbf{c}_q \cdot \nabla$.

All the particle-particle interactions generated by H' (from 2-body up to Q-body interactions) can be mapped onto a local collision operator $\Omega_q(f_1 \ldots f_Q)$ at $\mathbf{x}$. In particular, for type-II quantum algorithms, the quantum entanglement is localized to those Q-qubits at $(\mathbf{x},t)$ and then this entanglement is spread throughout the lattice by unitary streaming[3,4]:

$$f_q'(\mathbf{x},t) = f_q(\mathbf{x},t) + \Omega_q(f_1 \ldots f_Q),\ f_q(\mathbf{x}+\Delta\mathbf{x}_q, t+\Delta t) = f_q'(\mathbf{x},t)\ . \quad (1)$$

Here f_q is the incoming probability and f_q' the outgoing probability. In the classical limit, there exists a fundamental discrete entropy function[1,2,5]

$$\mathbf{H}(f_1 \ldots f_Q) = \sum_{q=1}^{Q} f_q \ln(f_q / w)\ , \quad (2)$$

where the normalized weights $\left(\sum_q w_q = 1\right)$ are determined self-consistently. The collision operator Ω_q in Eq. (1) is determined so that one remains on a constant entropy surface

$$\mathbf{H}(f_1' \ldots f_Q') = \mathbf{H}(f_1 \ldots f_Q)\ . \quad (3)$$

Eqs. (1–3) constitute the basics of the detailed-balance lattice algorithms for fluid turbulence that are ideal for parallel (both classical and quantum) supercomputers.

In the Q-dimensional velocity space, the relaxation distribution function f_q^{eq} is determined analytically by extremizing the H-function subject to the local collisional constraints of conservation of probability and probability flux. f_q^{eq}, considered as a vector, is the bisector of the difference between the incoming and outgoing kinetic vectors in the inviscid limit $\lim_{\mu\to 0} \alpha/2\tau = 2$:

$$f_q = f_q^{eq} - \frac{2\tau}{\alpha}\Omega_q,\ f_q' = f_q^{eq} + \left(1 - \frac{2\tau}{\alpha}\right)\Omega_q \quad (4)$$

Eliminating Ω_q and f_q' from Eqs. (4) and (1) one obtains the LB equation

$$f_q(\mathbf{x}+\Delta\mathbf{x}_q, t+\Delta t) = f_q(\mathbf{x},t) + \frac{\alpha}{2\tau}\left[f_q^{eq}(\mathbf{x},t)\right] - f_q(\mathbf{x},t),\ q = 1 \ldots Q \quad (5)$$

This is basically the entropic LB[1,2] with the BGK collisional relaxation parameters $\alpha(\mathbf{x},t)/2\tau$ and f_q^{eq} determined from Eqs. (2) and (3). In the Chapman-Enksog limit, ($\Delta\mathbf{x} \to 0$, $\Delta t \to 0$)—and identifying the density and momentum moments $\sum_q f_q = \rho$, $\sum_q \mathbf{c}_q f_q = \rho\,\mathbf{u}$ —one recovers the quasi-incompressible Navier-Stokes equation with

$$\text{effective viscosity: } \mu(\mathbf{x},t) = \frac{1}{6}\left(\frac{4\tau}{\alpha(\mathbf{x},t)} - 1\right);$$
$$\text{molecular viscosity: } \mu_0 = \frac{1}{6}(2\tau - 1),\ \tau > 0.5 \quad (6)$$

To avoid discrete lattice geometry effects polluting the turbulence simulations, one is restricted to certain Q's on a cubic lattice. In particular it can be shown that on a unit cubic lattice, the lowest order kinetic velocity models are

Q15: rest velocity, speed 1 (6 velocities), speed $\sqrt{3}$ (8 velocities) – i.e., $Q = 15$

Q19: rest velocity, speed 1 (6 velocities), speed $\sqrt{2}$ (12 velocities) – i.e., $Q = 19$

Q27: rest velocity, speed 1 (6), speed $\sqrt{2}$ (12), and speed $\sqrt{3}$ (8) – i.e., $Q = 27$ (7)

Because detailed balance is in-built into the entropic LB algorithm [see Eq. (3)], the scheme is unconditionally stable for arbitrary large Reynolds numbers, Re = $U_0 L/2\pi\mu_0$.

3. CAP Parallelization and Simulation Results

Since entropic LB consists of local collisional relaxation and simple shifting of data along the lattice links, it is ideally parallelized. In the CAP-Phase I run,

we investigated the scaling of our entropic lattice Boltzmann (ELB)-Q27 algorithm on the Naval Oceanographic Office (NAVO) IBM-P5 (Babbage) all the way up to the full 2,912 PEs available, achieving over 6.3 teraflops (TFlops)/s sustained performance (see Figure 1). This is close to perfect scaling with the number of PEs. The MHD-LB code has been run on the Earth Simulator on 4,800 PEs, achieving a sustained timing of over 26 TFlops/s (which is 67% of peak on this vector machine)—the best performance of a scientific code on that supercomputer to date. On Blue Gene this code has been run on 32,768 PEs and achieving over 9.1 TFlops/s (23% of peak on this #PEs scalar machine), again with excellent scaling.

Table 1. GFlops/s per CPU for 2912 CPUs for 2,000 time-steps for the 3 ELB-codes

#PEs	Grid	Model	Wallclock (s)	GFlops/s per PE
2912	ca1950^3	ELB-Q27	7 554.7	2.17
2912	ca1950^3	ELB-Q19	5 602.7	2.24
2912	ca1950^3	ELB-Q15	4 798.4	2.05

In Table 1 we show the wallclock time and average performance of the various ELB models for the full 2,912 PEs available for 2,000 LB time-steps. The Q27 model, based on the 27 kinetic streaming vectors, is the most memory intensive (about 1 KB/grid point) and requires a wallclock time which is over 1.5 times that required by the Q15 model (which requires just 0.5 KB/grid point).

For CAP Phase II, we wished to investigate the role of the underlying kinetic lattice symmetry on Navier-Stokes turbulence, since all three ELB-algorithms recover the Navier-Stokes equations to leading order in the Chapman-Enskog expansion. This is particularly important since on small grids (e.g., 512^3) and low molecular viscosities ($\mu_0 = 2\times10^{-4}$) we[4] had found very minor differences in the simulation results from the Q27, Q19, and Q15 models. With 2,048 PEs available for 24 hour shifts, the maximal spatial grid for the Q27 algorithm was $1{,}600^3$. All three models were run with the same base parameters: $u_0 = 0.035$, $\mu_0 = 5\times10^{-4}$ on the $1{,}600^3$-grid (i.e., with a base Re $= u_0 L/2\pi\mu_0 \approx 18{,}000$ and computational resolution/grid spacing $\mathrm{Re}^{3/4}/L \approx 1$) for a Kida initial velocity profile[6] with delta-function energy spectra. In Figure 2, we plot the normalized kinetic energy $<|\mathbf{u}(\mathbf{x},t)|^2> / <|\mathbf{u}(\mathbf{x},0)|^2>$, the normalized enstrophy $<|\boldsymbol{\omega}(\mathbf{x},t)|^2> / <|\boldsymbol{\omega}(\mathbf{x},0)|^2>$, palinstrophy $2P(t) = <|\nabla\times\boldsymbol{\omega}|^2>$, where the vorticity $\boldsymbol{\omega} = \nabla \times \mathbf{u}$, and $< .. >$ represent volume average over the periodic domain. The ELB-dissipation rate $\varepsilon(t)$is defined by $\varepsilon(t) = 2\mu_{eff}(t)\langle S_{ij}S_{ij}\rangle$, where S_{ij} is the usual rate of strain tensor and the effective relaxation rate (to make an analogy with standard LB algorithms) $\mu_{eff}(t)=(<4\tau/\alpha(\mathbf{x},t)>-1)/6$. Clearly the Q19-results significantly deviates even qualitatively from the Q27- and Q15-results, while there is strong quantitative agreement between the Q27- and Q15- models (up to a simple rescaling). This contrasts strongly with a low-resolution grid run on 512^3 at a somewhat lower molecular viscosity, see Figure 2(f). It appears that these differences arise from the Newton-Raphson root finder that determines at each grid point and at each time the $\alpha(\mathbf{x},t)$ function that enforces detailed balance on the constant entropic surface, Eq. (3). These functions $\alpha(\mathbf{x},t)$ seem to be much more lattice dependent, i.e., whether Q27, Q19 or Q15, than would have been gleaned from small grid runs. In Figure 3, we plot the development of the longitudinal and transverse 1D energy spectra:

$$E_{long}(k_x,t) = \sum_{k_y,k_z}\left|v_x(\mathbf{k},t)^2\right|,\quad E_{trans}(k_x,t) = \sum_{k_y,k_z}\left|v_x(\mathbf{k},t)^2\right| \qquad (8)$$

for the initial Kida velocity profile with initial delta function spectra

$$E_{\sim}(k_\cdot,0) = E_\cdot\delta(k_\cdot-2),\ \text{and}\ E_{\_}(k_\cdot,0) = E_\cdot[\delta(k_\cdot-2)+\delta(k_\cdot-4)] \qquad (9)$$

While the terabytes of data from the early stages (t < 28K) of the Q27-run are being retrieved and analyzed, some of the data from the t ≥ 28K has been analyzed. The energy spectra approximately obey a $k^{-5/3}$ Kolmogorov law, with a slight upturn at the very large k_x in E_{long}, indicating that the run is slightly unresolved at these scales.

The probability distribution functions (pdfs) for the velocity and vorticity components are shown in Figure 4. The velocity field is basically Gaussian—but with tails that are substantially higher than a Guassian. These tails die out with time as seen by the plot of $P[v_x]$ at t = 29K (Figure 4a) and at t = 41K (Figure 4b). The pdfs for the other velocity components have very similar behavior. On the other hand, the vorticity pdf is well fitted by an exponential pdf. This is indicative of intermittency in the turbulence.

4. Turbulence Morphology for Free Shear Turbulence

There is a correlation between the onset of turbulence in a laminar-to-turbulence transition and the order-disorder phase transition in ferromagnetism. Just as Ising lattice models are fundamental to understanding critical phenomena, kinetic lattice gas models that we are pursuing could have a similar impact. We now give some preliminary results on the turbulence morphology from 512^3 grid runs. The morphology can be broken down into

three main stages, Figure 5. Stage 1 occurs in the initial time interval $0 < t < 3.2K$ with the enstrophy $\Omega(t)$ increases exponentially, independent of the viscosity. The enstrophy curve is plotted in Figure 5 with the integer dots '1'. '2' ... '7'—and these integers correspond to the isosurfaces of constant vorticity at t = 1K, t = 2K ... t = 7K in Figure 5. The color coding is based on the value of $\hat{\mathbf{u}} \cdot \hat{\boldsymbol{\omega}}$: grey corresponds to $\hat{\mathbf{u}} \cdot \hat{\boldsymbol{\omega}} =$ -, blue for $\hat{\mathbf{u}} \cdot \hat{\boldsymbol{\omega}} = +1$ and red for $\hat{\mathbf{u}} \cdot \hat{\boldsymbol{\omega}} = -1$. In this initial stage, the isosurfaces of vorticity are stretched with a sharp rise in $d\Omega/dt$ (the sharply rising curve above the enstrophy curve in Stage 1). In Stage 2, for time $3.2K < t < 9K$, shown shaded in Figure 5, there is large scale anisotropic turbulence with intermittency. In this shaded region $d\Omega/dt$ becomes jagged and predominantly is decreasing in large spurts with intermediate avalanches occurring at t = 5.1K, and 6.75K (vertical red lines in Stage 2 of Figure 5). Stage 3, for $9K < t < 14K$, is the inertial subrange with eventual exponential decay of the enstrophy (see curve fitted red line that fits $\Omega(t)$ well for $t > 10K$). In this Stage 3, we see the onset of homogeneous isotropic small scale turbulence with energy cascading to small scales leading to the $k^{-5/3}$ Kolmogorov energy spectrum. The velocity pdf is Gaussian while the vorticity pdf is exponential (see the inset plots in Figure 5).

5. Concluding Remarks

Using CAP resources we have been able to uncover lattice geometry effects in the entropic lattice Boltzmann algorithm that had not been expected from lower grid resolution runs. In the entropic formulation, one is working with a generalized BGK collision operator that has within it the germs of detailed balance. Thus, the unconditionally stable algorithm is achieved with a variable transport coefficient, not unlike Large Eddy Simulations (LES) in CFD. Indeed, we have explored this connection in some detail but will report those findings elsewhere due to space limitations here. Another unexpected result unearthed by the CAP runs was the dependence of the ELB on the Mach number. A low Mach number expansion has to be performed to analytically evaluate the Lagrange multipliers arising in the extremization of the H-function subject to local collisional constraints. We have found that the Q15-bit model is less sensitive to the flow Mach number than the Q27-bit model. Another somewhat unexpected finding was the importance of maintaining the distribution function correlations in the mesoscopic description. To perform the long-time $1{,}600^3$-grid runs we needed to perform continuation runs. In the early stages of CAP we tried to minimize the amount of input/output read-out/read-in and to reconstruct the relaxation distribution function from its moments rather than keeping the full correlation information. While this did not affect the energy decay, there were significant discontinuities introduced into the enstrophy and higher energy spectral moments.

The parallelization strength of ELB arises from the modeling of the macroscopic nonlinear derivatives by local moments. Chapman-Enskog asymptotics will then, on projecting back into physical space, yield these nonlinear derivatives. Indeed, this will allow ideally parallelized Smagorinsky type LES to be modeled by LB methods and in LB-MHD algorithms enforce automatically $\nabla \cdot \mathbf{B} = 0$ without the recourse to expensive divergence cleaning algorithms.

The interconnection between quantum algorithms that can run on quantum (and classical) computers and ELB (that can only run on classical computers) has been outlined as well as a new morphology of free shear turbulence and the onset of laminar-to-turbulence transition. The analogy between

Order-disorder phase transition	$\leftrightarrow$	(Lattice) Ising Model
laminar-turbulence fluid transition	$\Leftrightarrow$	Entropic Lattice Boltzmann Model

is being strongly pursued.

Acknowledgements

This work could only have been performed by using the CAP Phase II resources on NAVO's IBM-P5 as well as some resources from a special grant from the Department of Energy (DoE) on National Energy Research Supercomputer Center's (NERSC) IBM-P3. Parallelization help from Dr. Jonathan Carter, NERSC, is greatly appreciated as well as the assistance of John Skinner during the CAP runs. This work was supported by Air Force Research Laboratory, Air Force Office of Scientific Research and DoE.

References

1. Boghosian, B.M, .J. Yepez, P. Coveney, and A. Wagner, *Proc. Roy. Soc.*, A457, 717, 2001.

2. Karlin, I.V., A. Ferrante, and H.C. Ottinger, *Europhys. Lett.*, 47, 182, 1999.

3. Yepez, J., *Phys. Rev.*, E63, 046702, 2001.

4. Yepez, J., *Phys. Rev.*, A74, 042322, 2006.

5. Keating, B., G. Vahala, J. Yepez, M. Soe, and L. Vahala, *Phys. Rev.*, E75, 036712, 2007.

6. Kida, S. and Y. Murakami, *Phys. Fluids*, 30, 2030, 1987.

7. Goldenfeld, N., *Phys. Rev. Lett.*, 96, 044503, 2006.

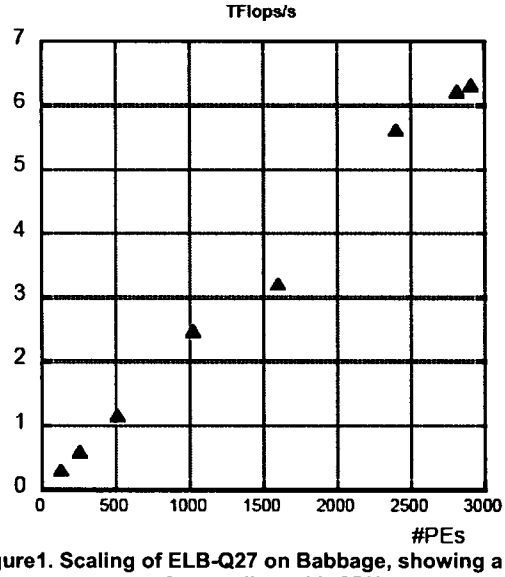

Figure1. Scaling of ELB-Q27 on Babbage, showing a near perfect scaling with CPUs

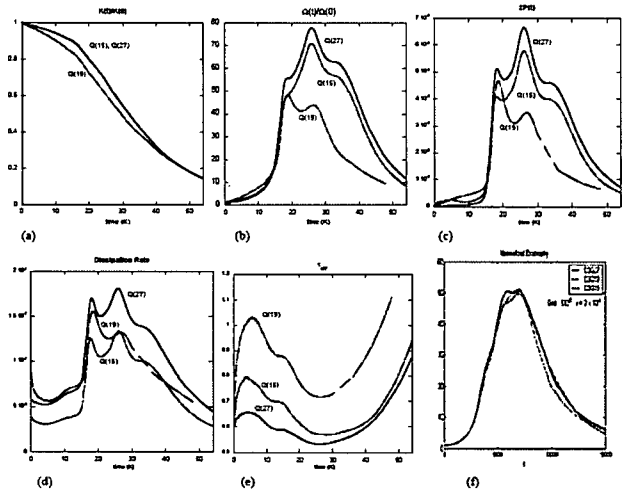

Figure 2. The evolution of the normalized (a) kinetic energy $K(t)/K(0)$, (b) enstrophy $\Omega(t)/\Omega(0)$,(c) palinstrophy $P(t)$, (d) dissipation rate $\varepsilon(t)$, (e) τ_{eff} for the Q27, Q19, and Q15 algorithms on $1{,}600^3$-grid with (f) normalized enstrophy from a 512^3-simulation at somewhat lower molecular viscosity

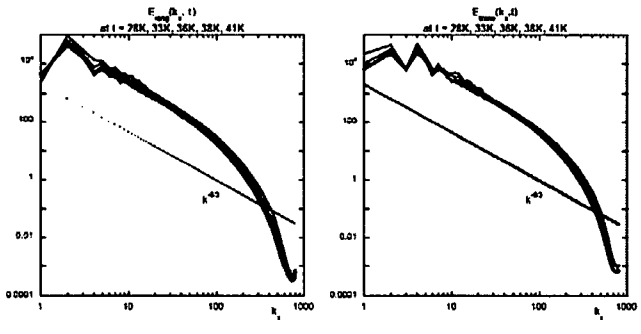

Figure 3(a). The longitudinal energy spectrum, (b) the transverse energy spectrum for t > 28K

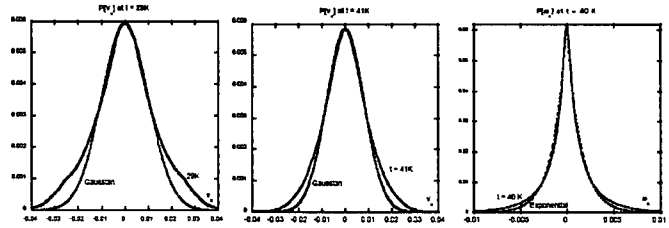

Figure 4. The pdf for the velocity component v_x at (a) t = 29K, and (b) t = 41K, fitted to Gaussian pdfs. The pdf for the vorticity component ω_x at t = 40K is shown in (c), fitted to an exponential pdf.

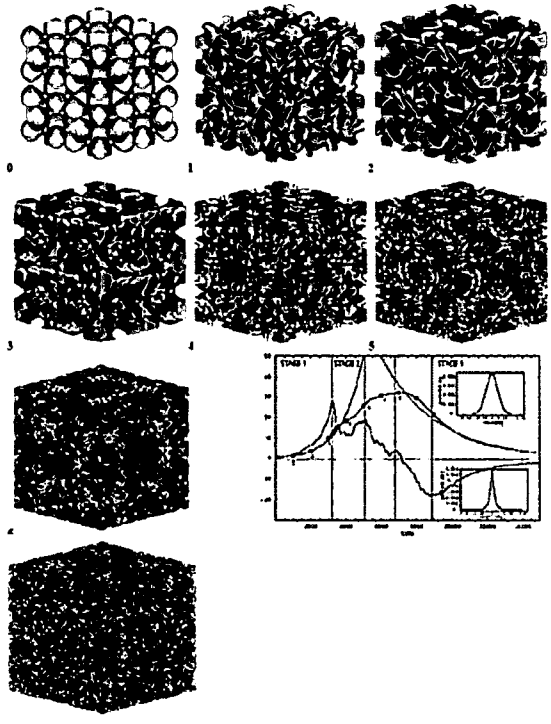

Figure 5. Surfaces of constant vorticity from t = 0K to t = 7K, color coded by $\hat{u} \times \hat{\omega}$ [grey = 0, blue = +1, red = −1]. Stage 1: 0< t < 3.2K. Vortex stretching, with an exponential growth in the enstrophy $\Omega(t)$ – the 1....7 corresponds to vorticity isosurface plots. Stage 2: 3.2K < t < 9K. Large scale anisotropic turbulence and intermittency occur. The major breaking points are at 3.2K, 5.1K and 6.8K (red lines in enstrophy plot). Stage 3: t > 9K. Inertial subrange with homogeneous isotropic small scale turbulence with $k^{-5/3}$ Kolmogorov energy.